Scalar dispersion by large eddy simulations and a Lagrangian stochastic subgrid model

Guoxin Wei, Ivana Vinkovic, L. Shao, Serge Simoëns

Scalar dispersion by a large-eddy simulation and a Lagrangian stochastic subgrid model

Guoxin Wei, Ivana Vinkovic,[a] Liang Shao, and Serge Simoëns
LMFA, UMR CNRS 5509, Université de Lyon I, Ecole Centrale de Lyon, INSA, 69131 Ecully Cedex, France

(Received 7 February 2006; accepted 17 July 2006; published online 5 September 2006)

A hybrid Eulerian-Lagrangian large-eddy simulation (LES) is used to compute scalar dispersion in a turbulent flow. Instead of resolving the passive scalar transport equation, fluid particles are tracked in a Lagrangian way. In order to obtain the subgrid scale velocity component of fluid particles, a Lagrangian stochastic subgrid model is coupled with the Eulerian LES. The Lagrangian stochastic subgrid model is written in terms of subgrid scale statistics. The coupling is applied to the study of turbulent scalar dispersion. The results of our simulation are compared with a direct numerical simulation and with experimental results. © *2006 American Institute of Physics*.
[DOI: 10.1063/1.2337329]

I. INTRODUCTION

Since the pioneering work of Deardorff,[1] large-eddy simulation (LES) has become a well established tool for computing turbulent flows,[2] as well as passive[3,4] or reactive[5,6] scalar dispersion. This approach is particularly interesting for the study of atmospheric dispersion of pollutants or for predicting instantaneous segregation. By means of LES the instantaneous evolution of large turbulent structures can be computed. These structures produce sweeping events responsible for scalar state far from the average field. However, pollution peaks or chemical reactions take place at a scale much smaller than the grid scale used in the LES. Therefore, the subgrid velocity fluctuations must be modeled separately.

In previous studies related to LES, scalar dispersion has been treated by resolving the large-scale transport equation for the concentration in a completely Eulerian approach[7,8] or by solving the filtered probability density function (PDF) equation.[9] In this work, Lagrangian tracking of fluid particles containing scalar is adopted. In order to obtain the small scale component of the velocity of fluid particles at a subgrid scale level, the Eulerian LES is coupled with a Lagrangian stochastic subgrid model. It should be noted that Gicquel *et al.*[10] used a global Lagrangian stochastic model to resolve the transport equation for the velocity filtered density function (VFDF).

In this study, the classical Langevin model[11] is written in terms of local subgrid statistics. This way, the Lagrangian stochastic subgrid model is entirely given by the quantities directly computed by the Eulerian LES. The efficiency of the coupling is tested in comparison to direct numerical simulation (DNS) results in the case of a homogeneous isotropic turbulence. The time evolutions of the Lagrangian velocity autocorrelation and fluid particle dispersion are presented. The Lagrangian time scale is computed as well. The computed quantities are compared with the DNS results and with the results of the LES without the Lagrangian stochastic subgrid model for two different subgrid scale models.

The interests of this study are double. First, by coupling the three-dimensional Lagrangian stochastic subgrid model with the hybrid Eulerian-Lagrangian LES the subgrid velocity of fluid elements is obtained. Therefore, by the method presented in this study the whole (large scale and subgrid scale) Lagrangian velocity field is predicted. Second, in order to study scalar mixing at different Schmidt numbers, a diffusion model is introduced.[12] Scalar dispersion is computed by the hybrid Eulerian-Lagrangian LES coupled with the Lagrangian stochastic subgrid model. The results are compared with the experiments of Huq and Britter[13] in homogeneous isotropic turbulence. Profiles of mean concentration, concentration variance and mass flux are presented. Computations with different Schmidt numbers are also included. Vinkovic *et al.*[14] used such a model for passive scalar spreading in a turbulent boundary layer. The agreement of the mean concentration field was good, but the authors never tested the behavior of the integral Lagrangian time scale or the influence of the Schmidt number. This is of fundamental interest for testing deeply the behavior of this model applied to passive scalar dispersion in homogeneous and isotropic turbulence.

The paper is organized as follows: The LES used in this study is presented in Sec. II. The Eulerian LES is then coupled with Lagrangian tracking of fluid particles and a Lagrangian stochastic subgrid model in Sec. III. In Sec. IV a diffusion model is included in order to compute scalar dispersion. The improvements obtained by the hybrid Eulerian-Lagrangian LES are shown in Sec. V where the results of the LES coupled with the Lagrangian stochastic subgrid model are compared to DNS results. In Sec. VI, the hybrid Eulerian-Lagrangian LES is applied to passive scalar dispersion in a homogeneous isotropic turbulence. The results are compared with the experimental profiles.[13] In order to reinforce the validity of the diffusion model an inhomogeneous

[a]Electronic mail: ivana.vinkovic@ec-lyon.fr

case is briefly presented in Sec. VII. Further discussions about the hybrid Eulerian-Lagrangian LES are summarized in Sec. VIII.

II. LARGE-EDDY SIMULATION

The governing equations resolved by the LES for an incompressible turbulence can be written as

$$\frac{\partial \tilde{u}_i}{\partial x_i} = 0,$$
$$\frac{\partial \tilde{u}_i}{\partial t} + \tilde{u}_j \frac{\partial \tilde{u}_i}{\partial x_j} = -\frac{1}{\rho}\frac{\partial \tilde{p}}{\partial x_i} + \nu \frac{\partial^2 \tilde{u}_i}{\partial x_j \partial x_j} - \frac{\partial \tilde{\tau}_{ij}}{\partial x_j}, \tag{1}$$

where ρ, ν, u_i, and p are the fluid density, molecular viscosity, fluid velocity, and pressure. x_i $(i=1,2,3)$ are the Cartesian coordinates. $\tilde{\tau}_{ij} = \widetilde{u_i u_j} - \tilde{u}_i \tilde{u}_j$ is the subgrid stress that needs to be modeled. The tilde $(\tilde{\cdot})$ denotes the filtering operation, given by

$$\tilde{u}_i = \int_\Omega u_i(x',t) G_\Delta(x-x')dx', \tag{2}$$

where Ω represents the spatial domain and Δ is the filter size. The subgrid eddy viscosity model of Cui *et al.*[15] is used. Details of this model may be found in Ref. 15. The subgrid stress is modeled by an eddy viscosity:

$$\tilde{\tau}_{ij} - \tilde{\tau}_{kk}\delta_{ij} = -2\nu_t \tilde{S}_{ij}, \tag{3}$$

where

$$\tilde{S}_{ij} = \frac{1}{2}\left(\frac{\partial \tilde{u}_i}{\partial x_j} + \frac{\partial \tilde{u}_j}{\partial x_i}\right) \tag{4}$$

is the strain rate tensor for the resolved scale turbulence. The subgrid eddy viscosity ν_t is given by[15]

$$\nu_t = \frac{-5 S_k D_{ll}^{1/2}}{8\dfrac{\overline{\tilde{S}_{ij}\tilde{S}_{ij}}}{D_{ll}}\xi - 30\dfrac{\partial D_{ll}/\partial \xi}{D_{ll}}}, \tag{5}$$

in which

$$D_{ll} = 2\overline{\tilde{u}_1^{\,2}} - 2\overline{\tilde{u}_1(x_1)\tilde{u}_1(x_1+\xi)}, \tag{6}$$

$$D_{lll} = 6\overline{\tilde{u}_1(x_1)\tilde{u}_1(x_1)\tilde{u}_1(x_1+\xi)}, \tag{7}$$

$$S_k = \frac{D_{lll}}{D_{ll}^{3/2}}. \tag{8}$$

S_k is the skewness of longitudinal velocity increment for resolved scale turbulence and the overline denotes Reynolds averaged statistics. This subgrid eddy viscosity model depends on the longitudinal displacement ξ, which is equal to the longitudinal mesh length in computation. This model does not explicitly depend on the filter, like Smagorinsky[16] or structure function models.[17]

In order to check the influence of the subgrid model on the coupling of the LES with the Lagrangian stochastic subgrid model, the subgrid model of Chollet and Lesieur[18] is also used. In this case, the eddy viscosity ν_t is given by[18]

$$\nu_t = 0.267\sqrt{\frac{E(k_c)}{k_c}}, \tag{9}$$

where k is the frequency, k_c is the spectral frequency at the cutoff, and $E(k)$ is the kinetic energy spectrum.

Periodical boundary conditions are used in the three directions. The velocity fluctuations are computed by a pseudospectral method. In the homogeneous case, the initial velocity fluctuation field is constructed following the method proposed by Rogallo[19] with the Comte Bellot[20] spectrum as the initial turbulent kinetic energy spectrum. In the inhomogeneous case, the initial conditions are obtained by the procedure developed by Shao.[21] The second order Runge-Kutta scheme is used in time advance and the CFL condition is satisfied.

III. LAGRANGIAN STOCHASTIC SUBGRID MODEL IN EULERIAN LES

Details of the coupling between the Eulerian LES and the Lagrangian stochastic subgrid model may be found in Refs. 22 and 14. Here, we will only give the main features. Fluid particles are tracked in a Lagrangian way. The position of fluid particles at each time step, is given by

$$\mathbf{x}_p(t) = \frac{d\mathbf{v}}{dt}. \tag{10}$$

In a turbulent flow, the velocity of fluid particles may be obtained by

$$v_i(t) = \tilde{u}_i(\mathbf{x}_p(t),t) + v_i'(t), \tag{11}$$

where v_i is the Lagrangian velocity of the fluid particle in the x_i direction and u_i is the Eulerian velocity of the fluid at the position $\mathbf{x}_p(t)$ of the fluid particle. The sign $(\tilde{\cdot})$ denotes the filtering operation. v_i' is the Lagrangian velocity fluctuation around the Eulerian large scale velocity $\tilde{u}_i$. In order to compute the movement of a fluid particle within a grid, a Langevin model is introduced:

$$dx_{p_i} = v_i dt,$$
$$dv_i = (\gamma_i + \alpha_{ij}(v_j - \tilde{u}_j(\mathbf{x}_p,t)))dt + \beta_{ij}\eta_j(t), \tag{12}$$

where $\eta_j(t)$ is an isotropic, Gaussian white noise with zero mean and variance dt, so that $\overline{\eta_i(t')\eta_j(t'')} = \delta_{ij}\delta(t'-t'')dt$. The velocity of each fluid particle at a given time t, is modeled by a deterministic part $\gamma_i + \alpha_{ij}v_j'$ and a completely random term $\beta_{ij}\eta_j(t)$. The coefficients α_{ij}, β_{ij}, and γ_i are determined by relating the subgrid statistical moments of $\mathbf{v}(t)$ to the filtered Eulerian moments of the fluid velocity. This is shown by the following analysis.

A local subgrid PDF (Ref. 23) $\mathcal{P}_\mathcal{L}(\mathbf{v};t)$ of the velocity $\mathbf{v}$ is defined upon all the statistical realizations given by the fluid elements within a grid. Since we assume that the couple $(\mathbf{x}_p,\mathbf{v})$ is Markovian, the evolution of $\mathcal{P}_\mathcal{L}(\mathbf{v};t)$ is given by a Fokker-Planck equation:

$$\frac{\partial \mathcal{P}_{\mathcal{L}}(\mathbf{v};t)}{\partial t} = -\frac{\partial}{\partial v_l}[(\gamma_l + \alpha_{lq}(v_q - \tilde{u}_q))\mathcal{P}_{\mathcal{L}}(\mathbf{v};t)] + \frac{1}{2}\frac{\partial^2}{\partial v_l \partial v_q}(\beta_{lk}\beta_{qk}\mathcal{P}_{\mathcal{L}}(\mathbf{v};t)). \quad (13)$$

By integrating Eq. (13) over $\mathbf{v}$, the time evolution equations of all the statistical moments of $\mathbf{v}$ can be obtained:

$$\widetilde{v_{i_1}\cdots v_{i_n}}(t) = \int_{\mathbb{R}^3} v_{i_1}\cdots v_{i_n}\mathcal{P}_{\mathcal{L}}(\mathbf{v};t)dv_v. \quad (14)$$

The sign $\widetilde{(\cdot)}$ represents here an average taken over the statistical realizations given by all the fluid elements within the grid. The statistical average is equal to the spatial filtering operation used in the LES. With Eqs. (14) and (13) we obtain

$$\frac{d\tilde{v}_i}{dt} = \gamma_i + \alpha_{iq}(\tilde{v}_q - \tilde{u}_q), \quad (15)$$

$$\frac{d\widetilde{v_i v_j}}{dt} = \gamma_i\tilde{v}_j + \gamma_j\tilde{v}_i + \alpha_{iq}(\widetilde{v_j v_q} - \tilde{v}_j\tilde{u}_q) + \alpha_{jq}(\widetilde{v_i v_q} - \tilde{v}_i\tilde{u}_q) + \beta_{ik}\beta_{jk}. \quad (16)$$

By the LES, the Eulerian filtered moments of $\tilde{u}_i$ can be computed. In order to determine α_{ij}, β_{ij}, and γ_i, at a given time t_0 and position $\mathbf{x}^{(m)}$, the Lagrangian quantities $\tilde{v}_i$ and $\widetilde{v_i v_j}$ are assumed to be equal to the corresponding Eulerian quantities. Here, we proceed in analogy with van Dop *et al.*,[24] who developed this approach for determining the coefficients of the stochastic model in the case of a Reynolds averaged decomposition. After applying the filtering operation to the Navier-Stokes equations [Eqs. (1)], knowing that the subgrid turbulence is assumed homogeneous and isotropic, we obtain

$$\alpha_{ij} = \frac{3\delta_{ij}}{2\tilde{E}(\mathbf{x}^{(m)},t_o)}\left(\frac{1}{3}\frac{d\tilde{E}}{dt} - \frac{C_0\tilde{\varepsilon}}{2}\right)_{(\mathbf{x}=\mathbf{x}^{(m)},t=t_o)}, \quad (17)$$

$$\beta_{ik} = \sqrt{C_0\tilde{\varepsilon}(\mathbf{x}^{(m)},t_o)}\,\delta_{ik}, \quad (18)$$

$$\gamma_i = \left(\frac{\partial\tilde{u}_i}{\partial t} + \frac{\partial(\tilde{u}_i\tilde{u}_j)}{\partial x_j} + \frac{\partial\tau^r_{ij}}{\partial x_j}\right)_{(\mathbf{x}=\mathbf{x}^{(m)},t=t_o)}, \quad (19)$$

where $\tilde{E}$ is the subgrid turbulent kinetic energy, C_0 is the constant of Kolmogorov, and $\tilde{\varepsilon}$ the dissipation rate of subgrid turbulent kinetic energy. Under these considerations, the velocity of fluid elements given by the Lagrangian stochastic subgrid model writes as

$$dv_i = \left[\frac{\partial\tilde{u}_i}{\partial t} + \frac{\partial(\tilde{u}_i\tilde{u}_j)}{\partial x_j} + \frac{\partial\tau_{ij}}{\partial x_j} + \frac{3}{2}\frac{v_i - \tilde{u}_i}{\tilde{E}}\left(\frac{1}{3}\frac{d\tilde{E}}{dt} - \frac{C_0\tilde{\varepsilon}}{2}\right)\right]dt + \sqrt{C_0\tilde{\varepsilon}}\,\delta_{ij}\eta_j(t)dt. \quad (20)$$

Each fluid particle has a large scale and a subgrid scale velocity component. The large-scale velocity of the fluid particle is directly computed by the LES. The subgrid scale velocity component is obtained from the subgrid scale closure. It should be noted that the subgrid scale velocity v_i' has no influence on the large scale velocity field, $\tilde{v}_i$ computed by the LES. Therefore, $\widetilde{v_i v_i'} = 0$.

IV. THE SCHMIDT NUMBER EFFECT

In order to take diffusion into account a deterministic, continuous in time pairing particle exchange model is used. A full description of this model can be found in Refs. 25 and 12. We will give here only the main aspects.

The domain is divided in boxes that are small compared to the length scale of the flow.[26] In each box, at each time step, particles are randomly selected by pairs. For each pair (m,n), the particle concentrations $c_m(t)$ and $c_n(t)$ will evolve according to

$$\frac{dc_m(t)}{dt} = \psi(c_n(t) - c_m(t)), \qquad \frac{dc_n(t)}{dt} = \psi(c_m(t) - c_n(t)). \quad (21)$$

ψ is a relaxation coefficient. From a theoretical analysis ψ is chosen so that the PDF p_c of the concentration tends to a Gaussian function in isotropic turbulence. As suggested by Spalding,[27] ψ can be expressed as $\psi = \xi/T_{\text{diff}}$, where ξ is a random number between -1 and 1, and the diffusion time T_{diff} can be written as $T_{\text{diff}} = T/C_{\text{diff}}$, with C_{diff} the model coefficient and T the time scale of the velocity fluctuations defined as $T = E/\varepsilon$. In analogy with this formulation, we used the corresponding subgrid values $\tilde{E}$ and $\tilde{\varepsilon}$.

Pope[26] explained that C_{diff} has to be adjusted with the relaxation of the standard deviation of the concentration level σ_c. Even though Pope[26] suggested a value of 2, Michelot[25] proposed a value of 2.25 as more appropriate. C_{diff} depends on the Reynolds and the Schmidt number. However, there is no available model for C_{diff} covering a wide range of Reynolds and Schmidt numbers. In this study, we adopt two different values for C_{diff}, based on the experimental results of Huq and Britter.[13] In homogeneous isotropic turbulence a value of 2 is used in the case of a moderate Schmidt number (Sc=7). For the higher Schmidt number case (Sc=700), $C_{\text{diff}}=4$ is adopted. It will be shown at the end of the paper that these values for C_{diff} are valid as well for the case of an inhomogeneous shearless turbulence mixing layer. This indicates that C_{diff} depends on the Schmidt number but that C_{diff} is constant for a fixed Schmidt number and does not have to be tuned according to the level of inhomogeneity of the studied flow.

V. FLUID PARTICLE DISPERSION IN HOMOGENEOUS ISOTROPIC TURBULENCE

The aim of this work is to study Lagrangian diffusion and dispersion of species by a hybrid Eulerian-Lagrangian LES. In scalar diffusion or dispersion, velocity decorrelation time scales play a crucial role. These decorrelation time scales are given by Eulerian and Lagrangian velocity correlations as well as the integral time scale. In order to estimate the impact of the coupling, these quantities will be computed by means of DNS, LES and LES with the Lagrangian sto-

TABLE I. Characteristic parameters for the homogeneous isotropic turbulence test case.

Grids in LES	64^3 and 32^3
Grids in DNS	256^3
Turbulent kinetic energy	$E=460\ \mathrm{cm}^2/\mathrm{s}^2$
Turbulent dissipation rate	$\varepsilon=1000\ \mathrm{cm}^2/\mathrm{s}^3$
Kinematic viscosity	$\nu=1.5\times10^{-5}\ \mathrm{m}^2/\mathrm{s}$
Lagrangian integral time scale	$T_L=0.129$ s
Eulerian integral time scale	$T_E=0.243$ s
Reynolds number	$\mathrm{Re}_\lambda=94$

chastic subgrid model. In the DNS, the Lagrangian velocity is obtained from the Eulerian velocity field by a sixth-order Lagrange polynomial interpolation scheme.[28] In the LES, the large-scale Lagrangian velocity is obtained from the Eulerian velocity field by the same interpolation scheme while the subgrid scale Lagrangian velocity component is computed by the Lagrangian stochastic subgrid model. We will study the case of a homogeneous isotropic turbulence, and we will briefly present an inhomogeneous case in order to reinforce the validity of the diffusion model. The characteristic parameters of the computed flow are given in Table I.

In homogeneous, isotropic and stationary turbulence, the Lagrangian velocity autocorrelation can be defined as

$$R_L(\tau)=\frac{\overline{v_i(0)v_i(\tau)}}{\sqrt{\overline{v_i(0)^2}}\sqrt{\overline{v_i(\tau)^2}}}, \tag{22}$$

where $v_i(0)$ and $v_i(\tau)$ are the Lagrangian velocities of a fluid particle at the initial time $t=0$ of their release in the flow, and the time τ, respectively.

Figure 1 illustrates the time evolution of the $R_L(\tau)$ obtained by the DNS and by two LES with different resolutions. In this case, the LES was done with the subgrid model of Chollet and Lesieur.[18] The lower resolution case was computed with 32^3 nodes and the higher resolution with 64^3. As expected, when the resolution of the LES increases, the time evolution of $R_L(\tau)$ becomes closer to the one obtained by the DNS. Differences appear at short times and they are more pronounced when the LES resolution is lower. This was previously noticed by He *et al.*[29,30]

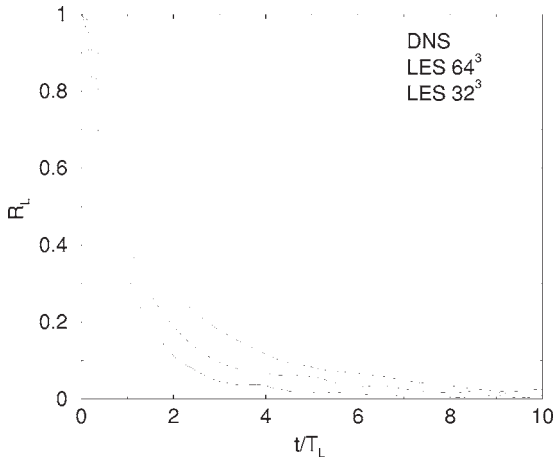

FIG. 1. Lagrangian velocity autocorrelation $R_L(\tau)$, $\mathrm{Re}_\lambda=94$. —, DNS; ---, LES 64^3; — — —, LES 32^3.

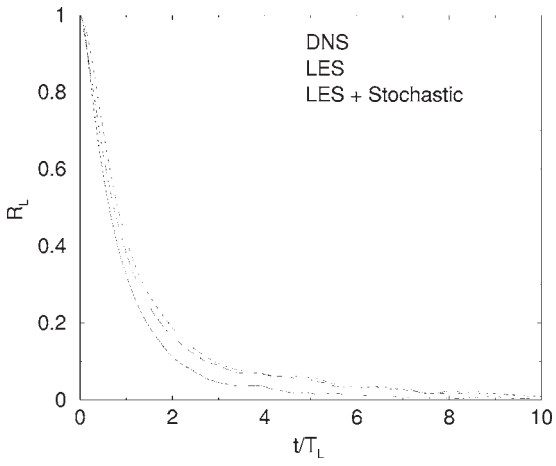

FIG. 2. Lagrangian velocity autocorrelation $R_L(\tau)$, subgrid scale model of Chollet and Lesieur (Ref. 18) —, DNS; ---, LES 64^3; — — —, LES 64^3 coupled with the Lagrangian stochastic subgrid model.

In Fig. 2 the time evolution of $R_L(\tau)$ obtained by a LES coupled with the Lagrangian stochastic subgrid model is compared to the DNS and a LES without the coupling. The results were computed with the subgrid scale model of Chollet and Lesieur.[18] Figure 3 is a zoom of Fig. 2 at short times. The difference between the LES and DNS appears most clearly at short times, Fig. 3. When the Lagrangian stochastic subgrid model is introduced, the error is reduced and the time evolution of $R_L(\tau)$ is closer to the one obtained by the DNS. However, at very short times, the Lagrangian stochastic subgrid model underpredicts the Lagrangian time correlation. The stochastic subgrid model introduces a velocity decorrelation for $t\to0$. This problem could be resolved by introducing a second-order stochastic equation as suggested by Sawford.[31]

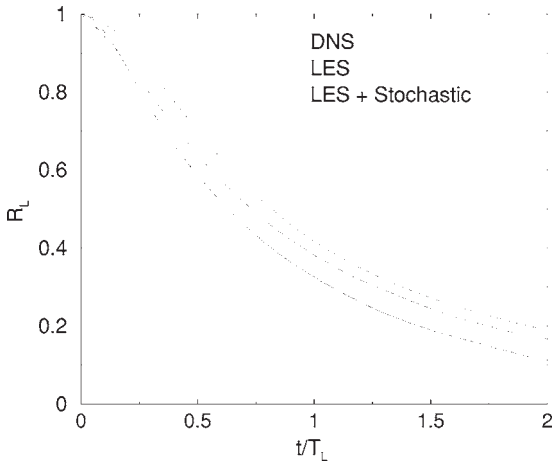

FIG. 3. Short time evolution of the Lagrangian velocity autocorrelation $R_L(\tau)$, subgrid scale model of Chollet and Lesieur (Ref. 18) —, DNS; ---, LES 64^3; — — —, LES 64^3 coupled with the Lagrangian stochastic subgrid model.

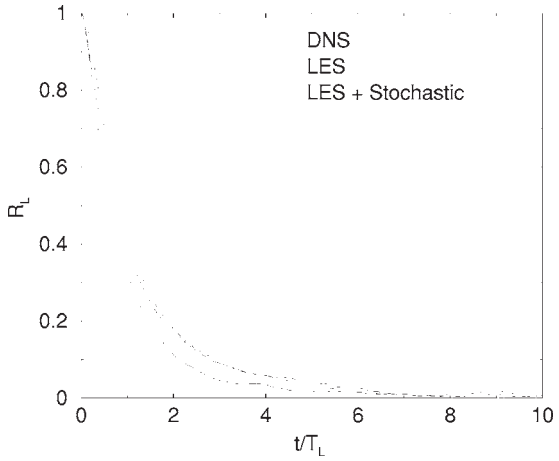

FIG. 4. Lagrangian velocity autocorrelation $R_L(\tau)$, subgrid scale model of Cui *et al.* (Ref. 15) —, DNS; ---, LES 64^3; — — —, LES 64^3 coupled with the Lagrangian stochastic subgrid model.

Figures 4 and 5 illustrate the same time evolution as Figs. 2 and 3, except that here, we used the LES subgrid model of Cui *et al.*[15] The improvements achieved by introducing the Lagrangian stochastic subgrid model are particularly noticeable at short times. By coupling the LES with the Lagrangian stochastic subgrid model, a better estimation of $R_L(\tau)$ is obtained. This improvement is independent of the subgrid model. The Lagrangian stochastic subgrid model introduces a random component which reproduces closer the turbulent statistics of small scales. Doing so, the reconstructed Lagrangian velocity field possesses a better autocorrelation.

The integral Lagrangian time scale T_L, is obtained by integrating $R_L(\tau)$ according to

$$T_L = \int_0^\infty R_L(t)dt. \tag{23}$$

Values of T_L obtained from Eq. (23) are shown in Table II for a resolution of 64^3 and 32^3. By introducing the Lagrangian stochastic subgrid model there is an improvement of 10% when T_L is obtained by integration [Eq. (23)]. For particular use, T_L can also be approximated from the turbulent kinetic energy E, the dissipation rate ε, and C_0, by[25]

$$T_L = \frac{4E}{3C_0\varepsilon}. \tag{24}$$

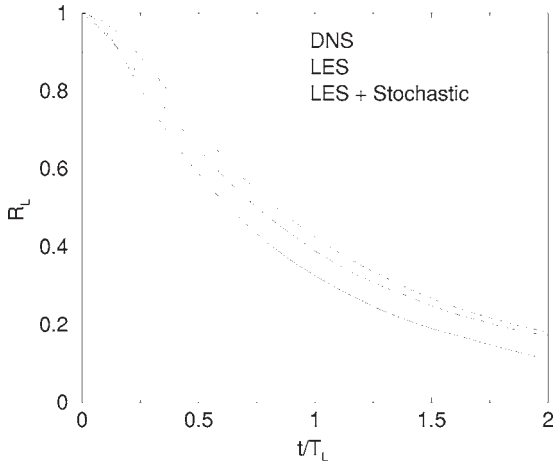

FIG. 5. Short time evolution of the Lagrangian velocity autocorrelation $R_L(\tau)$, subgrid scale model of Cui *et al.* (Ref. 15) —, DNS; ---, LES 64^3; — — —, LES 64^3 coupled with the Lagrangian stochastic subgrid model.

TABLE II. Lagrangian integral time scale T_L computed by the DNS, the LES and the LES coupled with the Lagrangian stochastic subgrid model. CL, subgrid scale model of Chollet and Lesieur (Ref. 18); CS, subgrid scale model of Cui *et al.* (Ref. 15).

	T_L [Eq. (23)]	T_L [Eq. (24)]
DNS	0.129	0.136
LES 64^3 CL[a]	0.156	0.128
LES 64^3 CS[b]	0.154	0.129
LES 64^3 CL[a] with stochastic model	0.144	0.143
LES 64^3 CS[b] with stochastic model	0.145	0.142
LES 32^3 CL[a]	0.206	
LES 32^3 CS[b]	0.172	
LES 32^3 CL[a] with stochastic model	0.177	
LES 32^3 CS[b] with stochastic model	0.153	

[a]Reference 18.
[b]Reference 15.

As we can see from Table II the improvement is less noticeable if T_L is obtained by Eq. (24). However, here the influence of the modeling and particularly of C_0 is not clear.[32] The comparison with the help of Eq. (24) is not a factor of validity of the hybrid Eulerian-Lagrangian LES. It only points out that this type of modeling can sustain for practical use Eq. (24). As the resolution of the LES decreases, whatever the subgrid scale model, the improvement achieved by coupling with the Lagrangian stochastic subgrid model becomes around 25%, if T_L is obtained by Eq. (23). The Lagrangian stochastic subgrid model induces the subgrid fluctuations that are necessary for recovering the statistical coherence of the scales at the subgrid level. This implies a lower value of T_L which is closer to the value obtained from the DNS. The correction achieved by the Lagrangian stochastic subgrid model is bigger when the resolution of the LES is smaller.

The influence of the Lagrangian stochastic subgrid model on fluid particle dispersion has been tested. Fluid particle dispersion may be defined by

$$\bar{X}(t) = \sqrt{\overline{(x_p(t;t_0,x_p(t_0)) - x_p(t_0))^2}}, \tag{25}$$

where $x_p(t_0)$ is the initial position of the fluid particle and $x_p(t;t_0,X(t_0))$ is the position of fluid particles at time t that were at $x_p(t_0)$ at t_0. The classical analysis,[33] predicts $\bar{X}(t)$ will evolve according to

$$\bar{X}(t) \to \sigma_u t \quad \text{for } t \ll T_L, \tag{26}$$

$$\bar{X}(t) \to \sigma_u\sqrt{2T_L t} \quad \text{for } t \gg T_L, \tag{27}$$

where $\sigma_u^2 = 2E/3$. The time evolutions of $\bar{X}(t)$ obtained by LES and by LES with the Lagrangian stochastic subgrid model are shown in Fig. 6, together with the classical evo-

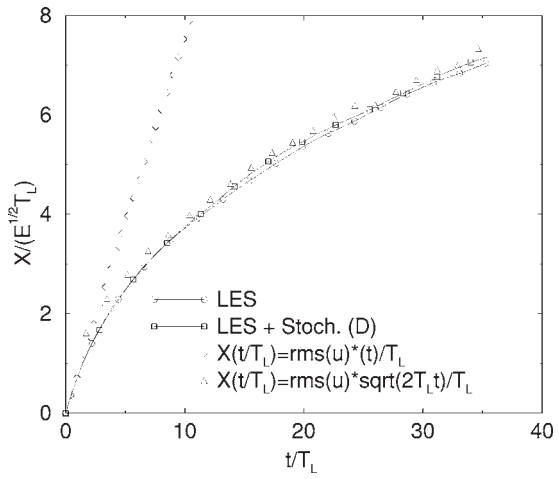

FIG. 6. Fluid particle dispersion, $\bar{X}(t)$. □, LES. ○, LES with Lagrangian stochastic subgrid model. ×, $\bar{X}(t)\rightarrow\sigma_u t$. +, $\bar{X}(t)\rightarrow\sigma_u\sqrt{2T_L t}$.

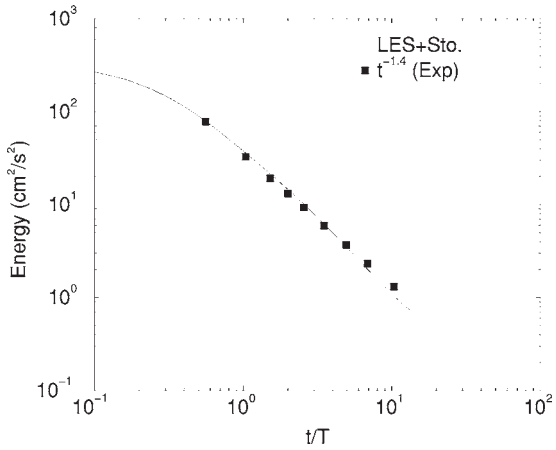

FIG. 7. Time evolution of total turbulent kinetic energy. —, LES 32^3 with the subgrid scale model of Cui *et al.* (Ref. 15) ■, Eq. (28).

lutions [Eq. (26)].[33] At short times, the mean dispersion of fluid particles is not strongly influenced by the Lagrangian stochastic subgrid model. At large times, it seems that by introducing the Lagrangian stochastic subgrid model a better approach of $\bar{X}(t)=\sigma_u\sqrt{2T_L t}$ is reached.

VI. PASSIVE SCALAR DISPERSION IN HOMOGENEOUS ISOTROPIC TURBULENCE

In this section the coupling between the Eulerian LES, the Lagrangian stochastic subgrid model and the diffusion model is applied to passive scalar dispersion. We computed the experimental test case of Huq and Britter,[13] who studied the dispersion of a passive scalar in a shear-free decaying grid-generated turbulence. The main characteristics of the experiment are given in Table III. More details on how to obtain the concentration statistics can be found in Ref. 14.

In this section, we use the subgrid scale model of Cui *et al.*[15] for the LES. Since the Reynolds number is very low, a 32^3 numerical resolution is used in LES.

The decay of the turbulent velocity fluctuations from the grid is presented in Fig. 7. The decay curves obtained by our LES with 32^3 grid points and with the subgrid scale model of Cui *et al.*,[15] are of the form

$$\frac{\overline{u_i'^2}}{\bar{U}^2}=A\left(\frac{x}{M}-4\right)^n \quad n\simeq -1.4, \tag{28}$$

where u_i' is the ith fluctuation velocity component, x the distance from the turbulence grid and A equals 0.07 and 0.05 for u_1' and u_3', respectively. This is in agreement with the reported grid-turbulence data of Huq and Britter.[13] Since the Re_λ is low, good accordance is achieved even though the resolution of the LES is not high.

Mean concentration profiles $\bar{C}$, for Sc=700, at different distances from the turbulence grid are presented in Figs. 8 and 9. The mean concentration has been normalized by its maximum value $\bar{C}_{\max}$, while the vertical coordinate z, has been normalized by the half-width of the scalar interface H, given by

$$H=\frac{\Delta C}{\left(\frac{dc}{dz}\right)_{z=0}}, \tag{29}$$

where ΔC is the initial concentration difference. Figures 8 and 9 correspond, respectively, to $x=7\lambda$ and $x=15\lambda$, λ being the Taylor microscale. At both distances, the mean concentration profiles obtained by our model are in good agreement with the experimental results. Close to the source (Fig. 8), the Lagrangian stochastic subgrid model has less impact on the mean concentration profile than further away from the

TABLE III. Characteristics of the flow in the experiment of Huq and Britter (Ref. 13).

Grid size	$M=0.64$ cm
Mean flow velocity	$\bar{U}=7.7$ cm/s
Reynolds number	$\mathrm{Re}_\lambda=15$
Schmidt number	Sc=7–700

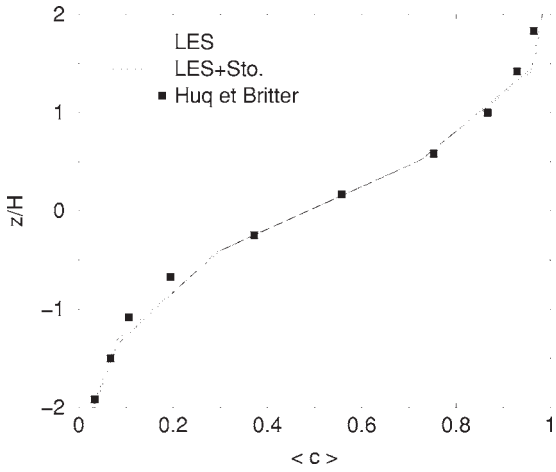

FIG. 8. Mean concentration profile $\bar{C}$, for Sc=700, at $x=7\lambda$. —, LES; ---, LES with Lagrangian stochastic subgrid model; ■, experimental profile of Huq and Britter (Ref. 13).

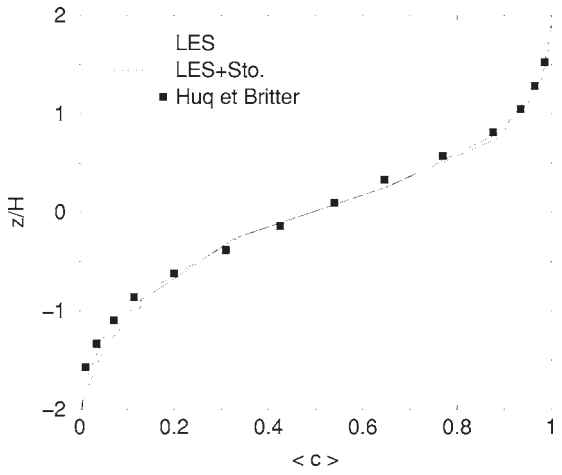

FIG. 9. Mean concentration profile $\bar{C}$, for Sc=700, at $x=15\lambda$. —, LES; ---, LES with Lagrangian stochastic subgrid model; ■, experimental profile of Huq and Britter (Ref. 13).

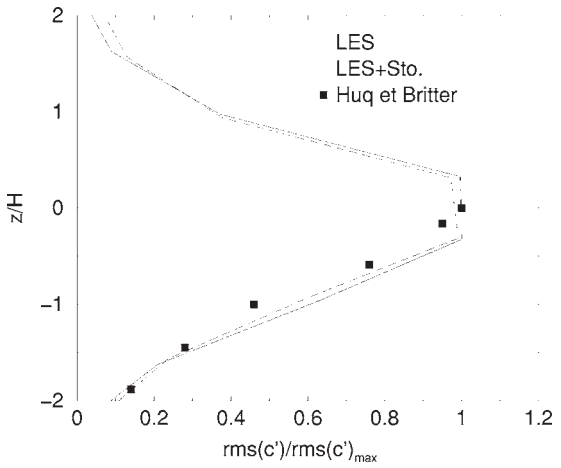

FIG. 11. Concentration fluctuation profile $\sqrt{\overline{c'^2}}$, for Sc=700, at $x=7\lambda$. —, LES; ---, LES with Lagrangian stochastic subgrid model; ■, experimental profile of Huq and Britter (Ref. 13).

source (Fig. 9). The improvements achieved by introducing the Lagrangian stochastic subgrid model are more significant in the regions of high concentration gradient.

Figure 10 illustrates the impact of the Schmidt number on the mean concentration profile at $x=15\lambda$. Two cases are computed Sc=7 and Sc=700. There is remarkable agreement between the computed and the experimental profiles, for both Schmidt numbers. Mean concentration profiles are not significantly affected by the Schmidt number, both in the experiments and in the computations.

Normalized concentration fluctuation profiles $\sqrt{\overline{c'^2}}$ are presented in Fig. 11 for Sc=700. The concentration fluctuation is normalized by its maximum value. The results from our computations are in good agreement with the experimental profiles. As we introduce the Lagrangian stochastic subgrid model, a slight improvement of the concentration fluctuation profile is obtained in the high gradient region. The evolution with distance from the turbulence grid of the concentration fluctuation profile is illustrated in Fig. 12. Good accordance is achieved with the corresponding experimental profiles. The results are also compared with a Gaussian profile:

$$\left(\frac{\overline{c'^2}(z)}{\overline{c'^2}_{\max}}\right)^{1/2} = e^{-(z/H)^2}, \tag{30}$$

showing consistency with the similarity theory of Gaussian dispersion. As for the mean concentration, Fig. 13 illustrates the impact of the Schmidt number on the concentration fluctuation profile at $x=15\lambda$. For both Schmidt numbers (Sc=7 and Sc=700) there is good agreement between the computed and the experimental profiles emphasizing that concentration fluctuation profiles are weakly affected by the Schmidt number.

The intensity of segregation, given by

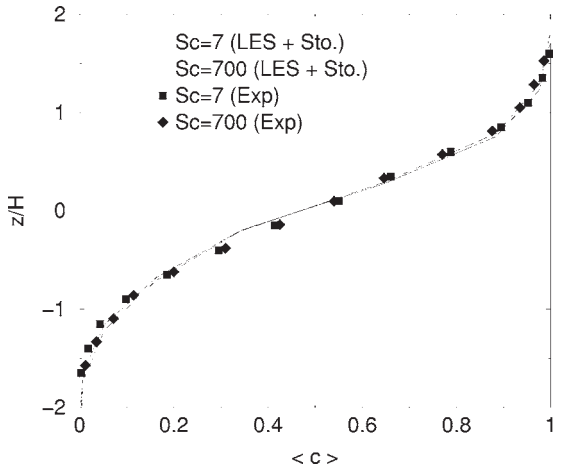

FIG. 10. Mean concentration profile $\bar{C}$, for Sc=7 and Sc=700, at $x=15\lambda$. —, LES with Lagrangian stochastic subgrid model Sc=7. ---, LES with Lagrangian stochastic subgrid model Sc=700. ■, Experimental profile of Huq and Britter (Ref. 13) Sc=7. ◆, Experimental profile of Huq and Britter (Ref. 13) Sc=700.

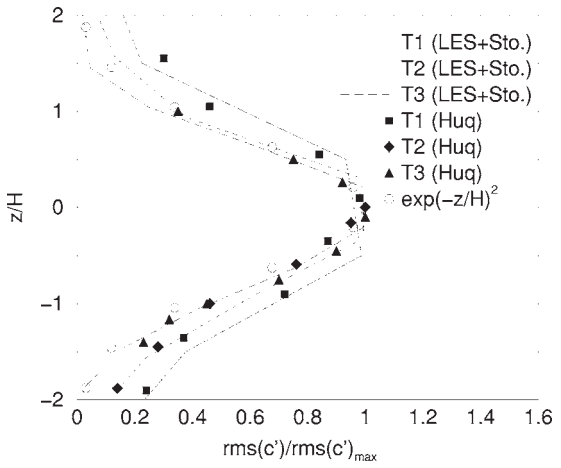

FIG. 12. Concentration fluctuation profile $\sqrt{\overline{c'^2}}$, for Sc=700, at $x=4\lambda$, $x=7\lambda$, and $x=15\lambda$. —, LES with Lagrangian stochastic subgrid model at $x=4\lambda$; ---, LES with Lagrangian stochastic subgrid model at $x=7\lambda$; — — —, LES with Lagrangian stochastic subgrid model at $x=15\lambda$. ■, Huq and Britter (Ref. 13) at $x=4\lambda$. ◆, Huq and Britter (Ref. 13) at $x=7\lambda$. ▲, Huq and Britter (Ref. 13) at $x=15\lambda$. ○, $e^{(-z/H)^2}$.

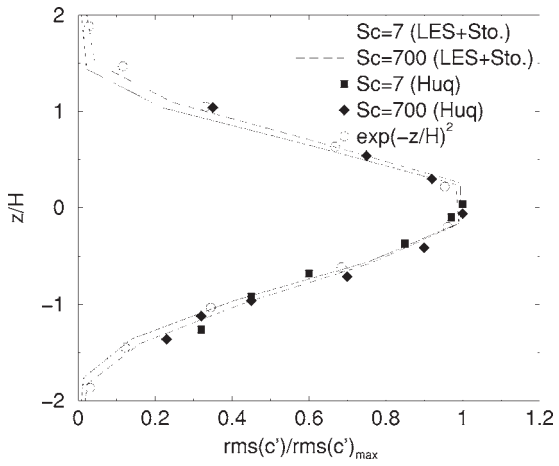

FIG. 13. Concentration fluctuation profile $\sqrt{\overline{c'^2}}$, for Sc=7 and Sc=700, at $x=7\lambda$. —, LES with Lagrangian stochastic subgrid model Sc=7. ---, LES with Lagrangian stochastic subgrid model Sc=700. ■, Experimental profile of Huq and Britter (Ref. 13) Sc=7. ◆, Experimental profile of Huq and Britter (Ref. 13) Sc=700. ○, $e^{(-z/H)^2}$.

$$Is = \frac{\overline{c'^2}}{\bar{C}(C_{\max} - \bar{C})}, \tag{31}$$

is also computed. In the experiment of Huq and Britter,[13] this measured parameter clearly shows the influence of the Schmidt number. *Is* varies from zero for a truly uniform mixture, and unity for a mixture without molecular mixing by definition. The effect of Sc on the uniformity is shown in Fig. 14. The more diffusive case (Sc=7) possesses a lower value of *Is* at the interface and approaches uniformity more rapidly. The effect of the Schmidt number is correctly predicted by our simulation together with the chosen set of values for the coefficient C_{diff}. This points out the dependence of C_{diff} on the Schmidt number and shows that our model correctly reproduces the influence of the diffusion process on the mean concentration (Fig. 10) and on the concentration fluctuations (Fig. 13) which results in the great effect of the diffusion process on the intensity of segregation (Fig. 14).

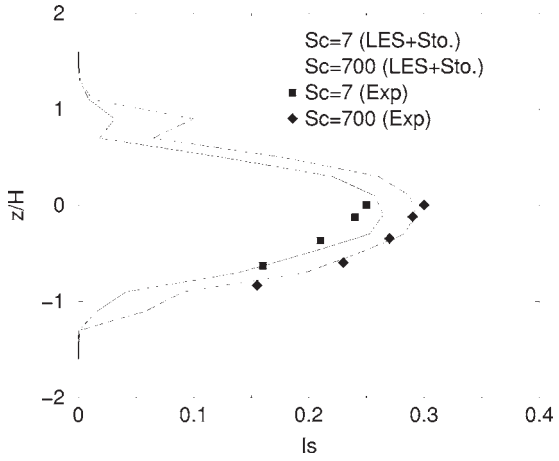

FIG. 14. Vertical profile of the intensity of segregation *Is*, for Sc=7 and Sc=700, at $x=15\lambda$. —, LES with Lagrangian stochastic subgrid model for Sc=7. ---, LES with Lagrangian stochastic subgrid model for Sc=700. ■, Huq and Britter (Ref. 13) for Sc=7. ◆, Huq and Britter (Ref. 13) for Sc=700.

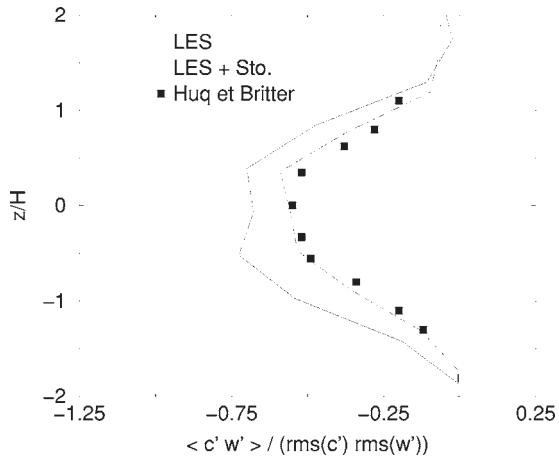

FIG. 15. Vertical profile of mass flux $\overline{c'u_3'}$, for Sc=700, at $x=15\lambda$. ——, LES; ---, LES with Lagrangian stochastic subgrid model. ■, Huq and Britter (Ref. 13).

Figure 15 shows the normalized flux profiles $\overline{c'u_3'}/\overline{c'u_3'}_{\max}$ at $x=15\lambda$ and for Sc=700. When the Lagrangian stochastic subgrid model is introduced the vertical profile is considerably improved. The impact of the Lagrangian stochastic subgrid model on this quantity is significant and without the coupling there would be an important error in the prediction. It is interesting to emphasize that with the approach presented in this study, second or higher order concentration statistics as well as mass flux can be obtained with no additional modeling assumptions.

VII. PASSIVE SCALAR DISPERSION IN INHOMOGENEOUS ISOTROPIC TURBULENCE

In this section, the different models developed are applied to passive scalar dispersion in an inhomogeneous isotropic turbulence without changing the value of C_{diff}. The computational results are compared with the experiments of Zhang[34,35] for a shearless turbulence mixing layer with passive scalar. The experiment consisted of two grid generated turbulences put side by side, along the transverse direction z. The bigger grid of size $M_2=5.0$ cm is put at $z=0$. The smaller grid of $M_1=2.5$ cm is put next. A passive scalar is emitted from the smaller grid. The characteristics of the experiment and the simulations are given in Table IV.

The Lagrangian integral time scale T_L is computed at different positions z along the direction of inhomogeneity.

TABLE IV. Characteristics of the experiment of Zhang (Refs. 34 and 35).

Grid size	$M_1=2.5$ cm
	$M_2=5.0$ cm
Mean flow velocity	$\bar{U}=300$ cm/s
Reynolds number	$\text{Re}_{\lambda_1}=21$
	$\text{Re}_{\lambda_2}=26$
Ratio of Taylor microscale	$\lambda_2/\lambda_1=1.27$
Ratio of turbulent kinetic energy	$E_2/E_1=2.48$
Schmidt number	$\text{Sc}=10^6$

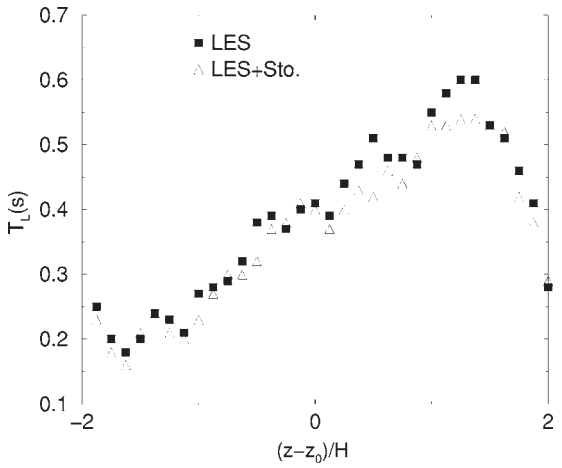

FIG. 16. Profiles of the Lagrangian integral time scale T_L in the direction of inhomogeneity, z. ■, LES without the stochastic model. △, LES with the stochastic model.

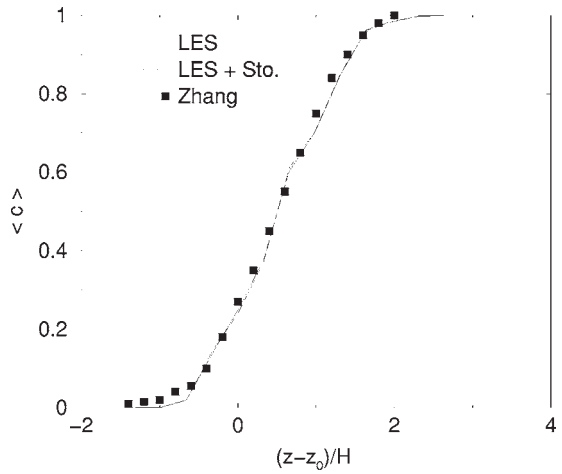

FIG. 18. Mean concentration profile $\bar{C}$, at $t=3T_\lambda$. —, LES. ---, LES with stochastic model. ■, Experimental profile of Zhang (Refs. 34 and 35).

The results obtained by the LES without the stochastic model and by the LES with the stochastic model are presented in Fig. 16. The transverse position z is normalized by H, the mixing width, and the zero is offset by z_0, the center of the mixing zone, given by

$$\left(\frac{d^2u(z)}{dz^2}\right)_{z_0}=0. \tag{32}$$

For small z, where the turbulent structures are large, T_L is small. As z increases, the Lagrangian integral time scale increases, attaining the maximum value in the region of quasihomogeneity of the small scales $(z-z_0)/H\rightarrow 2$.

Computed turbulent kinetic energy spectra, at different positions along the inhomogeneity direction z, are presented in Fig. 17. Different regions may be distinguished:

- z_1, the center of the quasihomogeneous turbulence region of the large grid ($M_2=5.0$ cm);
- z_2, the center of the quasihomogeneous turbulence region of the small grid ($M_1=2.5$ cm);
- z_3, the mixing region inside the large scale turbulence;
- z_4, the mixing region inside the small scale turbulence.

The energy of the mixing region is smaller than the energy of the large scale turbulence and higher than the energy of the small scale turbulence.

Once the shearless turbulence mixing layer is fully developed, fluid particles containing scalar are introduced into the domain. The mean concentration profile $\bar{C}$, obtained by our simulations and compared to the experimental results is presented in Fig. 18. There is good agreement between the computed profiles and the experimental results. There is practically no difference between the LES without the stochastic model and the LES with the stochastic model.

In Fig. 19, the computed and experimental profiles for the concentration fluctuation, $\sqrt{\overline{c'^2}}$ at $t=3T_\lambda$ are illustrated. Good agreement is achieved between our simulations and the experimental profiles, particularly in the highly inhomogeneous region $[-1<(z-z_0)/H<1]$. The time evolution of the concentration fluctuation profiles is presented in Fig. 20 illustrating the fact that the inhomogeneity and its time evolu-

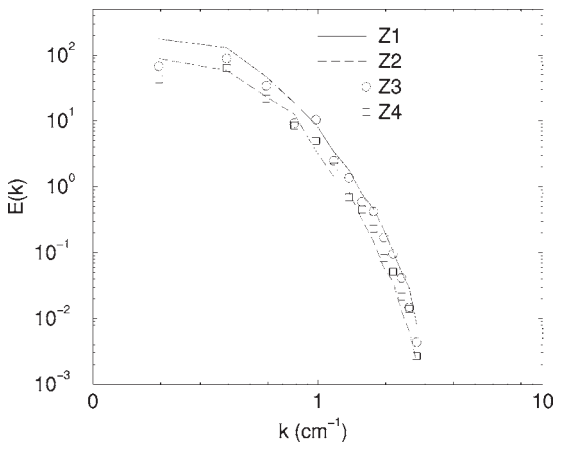

FIG. 17. Turbulent kinetic energy spectra at different z at $t=4T_\lambda$. —, z_1; ---, z_2; ○, z_3; □, z_4.

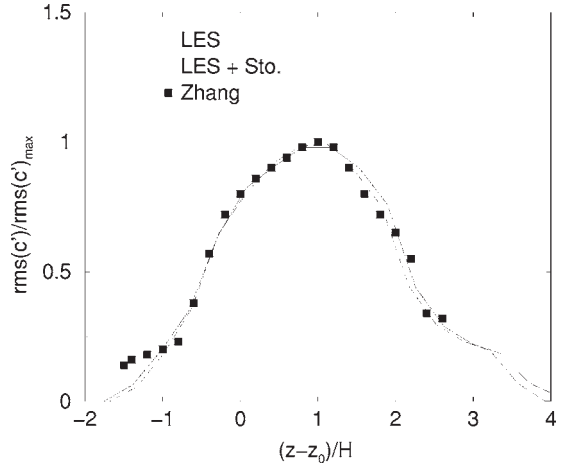

FIG. 19. Concentration fluctuation profile $\sqrt{\overline{c'^2}}$, at $t=3T_\lambda$. —, LES. ---, LES with stochastic model. ■, Experimental profile of Zhang (Refs. 34 and 35).

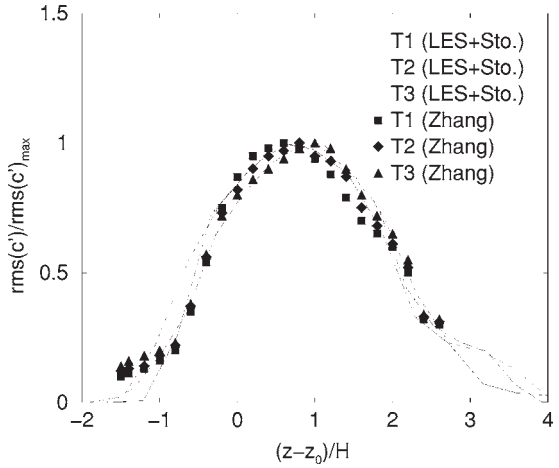

FIG. 20. Time evolution of the concentration fluctuation profile $\sqrt{\overline{c'^2}}$. —, LES with stochastic model at $t=3T_\lambda$. ---, LES with stochastic model at $t=4T_\lambda$. — — —, LES with stochastic model at $t=6T_\lambda$. ■, Experiment of Zhang (Refs. 34 and 35) at $t=3T_\lambda$. ◆, Experiment of Zhang (Refs. 34 and 35) at $t=4T_\lambda$. ▲, Experiment of Zhang (Refs. 34 and 35) at $t=6T_\lambda$.

tion are properly taken into account by our LES coupled with the Langevin model.

Finally, Fig. 21 illustrates the comparison between our computations and the experiments for the mass flux $\overline{c'u_3'}$, at different times ($t=3T_\lambda$, $t=4T_\lambda$, and $t=6T_\lambda$). Discrepancies appear in highly inhomogeneous region. However, we can consider that globally good agreement is achieved.

VIII. CONCLUSION

A hybrid Eulerian-Lagrangian LES is applied to the study of passive scalar dispersion in a turbulent flow. Fluid particles, containing scalar are tracked in a Lagrangian way. In order to obtain the Lagrangian subgrid velocity component of the tracked fluid elements, a Lagrangian stochastic subgrid model is coupled with the Eulerian LES. This hybrid Eulerian-Lagrangian LES allows the reconstruction of the whole high Reynolds number Lagrangian velocity field.

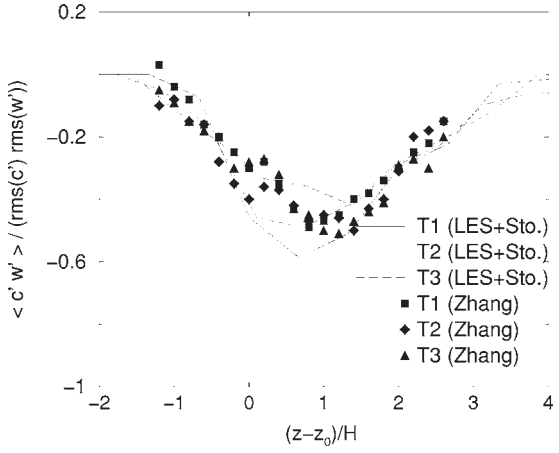

FIG. 21. Time evolution of the mass flux profile $\overline{c'u_3'}$. —, LES with stochastic model at $t=3T_\lambda$. ---, LES with stochastic model at $t=4T_\lambda$. — — —, LES with stochastic model at $t=6T_\lambda$. ■, Experiment of Zhang (Refs. 34 and 35) at $t=3T_\lambda$. ◆, Experiment of Zhang (Refs. 34 and 35) at $t=4T_\lambda$. ◆, Experiment of Zhang (Refs. 34 and 35) at $t=6T_\lambda$.

Lagrangian velocity correlations and the Lagrangian integral time scale computed by DNS, by LES and by LES with the Lagrangian stochastic subgrid model are compared. These results show that considerable improvement is achieved by introducing the Lagrangian stochastic subgrid model. By including the Lagrangian stochastic subgrid velocity, the statistical coherency at subgrid scale level is improved. The integral time scale is reduced, reaching closer the values obtained by the DNS. This result is enhanced when the spatial resolution of the LES decreases.

The coupling between the LES, the Lagrangian stochastic subgrid model and a diffusion model is applied to the study of passive scalar dispersion in a homogeneous isotropic turbulence. The results from our computations are compared with the experimental profiles of Huq and Britter.[13] Profiles of mean concentration, concentration fluctuations and mass fluxes are presented, illustrating good agreement with the experiments. By introducing the Lagrangian stochastic subgrid model the turbulent dispersion is improved. Particularly, the impact of the Lagrangian stochastic subgrid model on the mass flux is significant. In addition, the effect of the Schmidt number (Sc=7 and Sc=700) is properly captured by our simulation together with the chosen set of values for the diffusion coefficient C_{diff}.[25,12] This last result is confirmed for a high Schmidt number case ($\text{Sc}\sim 10^6$) of scalar mixing in an inhomogeneous shearless turbulence mixing layer. C_{diff} is clearly a function of the Schmidt number and in future work we will try to establish such a relationship.

With the hybrid Eulerian-Lagrangian LES, mass flux and segregation profiles can be obtain with no additional modeling assumptions. These quantities are of great importance when it comes to pollutant dispersion or chemical mixing problems. Higher order concentration statistics will be tested in the future to see how important the influence of diffusion modeling is on these quantities. This method could be applied widely to various problems of turbulent dispersion.

[1] J. W. Deardorff, "A numerical study of three-dimensional turbulent channel flow at large Reynolds numbers," J. Fluid Mech. **41**, 453 (1970).
[2] O. Métais and M. Lesieur, "Spectral large-eddy simulation of isotropic and stably stratified turbulence," J. Fluid Mech. **239**, 157 (1992).
[3] J. P. Chollet and M. Lesieur, "Modélisation sous-maille des flux de quantité de mouvement et de chaleur en turbulence tridimensionnelle isotrope," La Météorologie **6**, 183 (1982).
[4] R. I. Sykes and D. S. Henn, "Large-eddy simulation of concentration fluctuations in a dispersing plume," Adv. Electron. Electron Phys., Suppl. **26**, 3127 (1992).
[5] R. I. Sykes, D. S. Henn, and S. F. Parker, "Large-eddy simulation of a turbulent reacting plume," Atmos. Environ., Part A **26**, 2565 (1992).
[6] J. P. Meeder and F. T. M. Nieuwstadt, "Large-eddy simulation of the turbulent dispersion of a reactive plume from a point source into a neutral atmospheric boundary layer," Atmos. Environ. **34**, 3563 (2000).
[7] Z. Xie, P. Hayden, P. R. Voke, and A. G. Robins, "Large-eddy simulation of dispersion: Comparison between elevated and ground-level sources," J. Turbul. **5**, 1 (2004).
[8] S. S. Girimaji and Y. Zhou, "Analysis and modelling of subgrid scalar mixing using numerical data," Phys. Fluids **8**, 1224 (1996).
[9] X. Y. Zhou and J. C. F. Pereira, "Large-eddy simulation (2D) of a reacting plane mixing layer using filtered density function closure," Flow, Turbul. Combust. **64**, 279 (2000).
[10] L. Y. M. Gicquel, P. Givi, F. A. Jaberi, and S. B. Pope, "Velocity filtered density function for large eddy simulation of turbulent flows," Phys. Fluids **14**, 1196 (2002).
[11] D. J. Thomson, "Criteria for the selection of stochastic models of particle

trajectories in turbulent flows," J. Fluid Mech. **180**, 529 (1987).
[12] S. Simoëns, C. Michelot, M. Ayrault, and V. Sabelnikov, "Modèle stochastique de diffusion continu en temps: approximation différentielle de l'équation d'évolution de la densité de probabilité de la concentration et sa solution asymptotique dans le cas d'une turbulence homogène," C. R. Mec. **324**, 667 (1997).
[13] P. Huq and R. E. Britter, "Mixing due to grid-generated turbulence of a two-layer scalar profile," J. Fluid Mech. **285**, 17 (1995).
[14] I. Vinkovic, C. Aguirre, and S. Simoëns, "Large-eddy simulation and Lagrangian stochastic modeling of passive scalar dispersion in a turbulent boundary layer," J. Turbul. **7**, 1 (2006).
[15] G. Cui, H. Zhou, Z. Zhang, and L. Shao, "A new dynamic subgrid eddy vicosity model with application to turbulent channel flow," Phys. Fluids **16**, 2835 (2004).
[16] J. Smagorinsky, "Global atmospheric modeling and the numerical simulation of climate," in *Weather and Climate Modification* (Wiley, New York, 1974), p. 633.
[17] J. Bardina, J. H. Ferziger, and W. C. Reynolds, "Improved subgrid scale models for large-eddy simulation," AIAA Paper No. 801357.
[18] J. P. Chollet and M. Lesieur, "Parameterization for small scales of three dimensional isotropic turbulence using spectral closure," J. Atmos. Sci. **38**, 2747 (1981).
[19] R. S. Rogallo, "Numerical experiments in homogeneous turbulence," NASA Paper No. 81315 (1981).
[20] G. Comte-Bellot and S. Corrsin, "The use of contraction to improve the isotropy of grid generated turbulence," J. Fluid Mech. **25**, 657 (1966).
[21] L. Shao, "Etude d'une couche de mélange turbulente non cisaillée par simulation des grandes échelles," Ph.D. thesis, Ecole Centrale de Lyon (1992).
[22] I. Vinkovic, C. Aguirre, S. Simoens, and J. N. Gence, "Couplage d'un modèle stochastique lagrangien sous-maille avec une simulation grandes échelles," C. R. Mec. **333**, 325 (2005).
[23] A. W. Cook and J. J. Riley, "A subgrid model for equilibrium chemistry in turbulent flows," Phys. Fluids **6**, 2868 (1994).
[24] H. van Dop, F. T. M. Nieuwstadt, and J. C. R. Hunt, "Random walk models for particle displacement in inhomogeneous unsteady turbulent flows," Phys. Fluids **28**, 1639 (1985).
[25] C. Michelot, "Développement d'un modèle stochastique lagrangien: application à la dispersion et à la chimie de l'atmosphère," Ph.D. thesis, L'Ecole Centrale de Lyon (1996).
[26] B. S. Pope, "PDF methods for turbulent reactive flows," Prog. Energy Combust. Sci. **11**, 119 (1985).
[27] D. B. Spalding, "Concentration fluctuations in a round turbulent free jet," Chem. Eng. Sci. **26**, 95 (1971).
[28] J. I. Choi, K. Yeo, and C. Lee, "Lagrangian statistics in turbulent channel flow," Phys. Fluids **16**, 779 (2004).
[29] G.-W. He, R. Rubinstein, and L. Wang, "Effects of subgrid scale modeling on time correlations in large eddy simulation," Phys. Fluids **14**, 2186 (2002).
[30] G.-W. He, M. Wang, and S. K. Lele, "On the computation of space-time correlations by large-eddy simulation," Phys. Fluids **16**, 3859 (2004).
[31] B. L. Sawford, "Reynolds number effects in Lagrangian stochastic models of turbulent dispersion," Phys. Fluids A **3**, 1577 (1991).
[32] B. L. Sawford and P. K. Yeung, "Lagrangian statistics in uniform shear flow: Direct numerical simulation and Lagrangian stochastic models," Phys. Fluids **13**, 2627 (2001).
[33] A. S. Monin and A. M. Yaglom, *Statistical Fluid Mechanics* (MIT Press, Cambridge, 1971).
[34] X. H. Zhang, "Studies on passive scalar in shearless turbulent mixing layer," Ph.D. thesis, Tsinghua University (2002).
[35] X. H. Zhang, Z. S. Zhang, M. Ayrault, S. Simoëns, and F. Laadhari, "Experimental study on passive scalar diffusion in a turbulent shearless mixing-layer by Mie scattering diffusion and PIV," Proc. SPIE **5058**, 96 (2003).